Volume 1 | Number 1 | Jan 2013 | Pages 1–100

Journal of
Materials Chemistry A

Materials for energy and sustainability
www.rsc.org/materialsA

ROYAL SOCIETY
OF CHEMISTRY

ROYAL SOCIETY
OF CHEMISTRY

www.rsc.org/materialsA

Journal of Materials Chemistry A

ARTICLE

PREPARATION OF NARROWLY DISPERSED STEREOCOMPLEX NANOCRYSTALS: A STEP TOWARDS ALL-POLY(LACTIC ACID) NANOCOMPOSITES

R. Mincheva,[a] Ph. Leclère,[b] Y. Habibi,[a,c] J.-M. Raquez[a] and P. Dubois[a,*]

Stereocomplexed polylactide-based nanocrystals were designed through a two-stage procedure comprising (i) the stereocomplexation of enantiomeric polylactide-based triblock copolymers and (ii) their selective recovery after acid-hydrolysis of the amorphous blocks. A "one-pot" synthetic process to prepare two enantiomeric P(D,D-LA)-b-P(rac-LA)-b-P(D,D-LA) and P(L,L-LA)-b-P(rac-LA)-b-P(L,L-LA) triblock copolymers of $\overline{M}_n$ = 10,100 g/mol and Đ = 1.10-1.11 was developed via a two-step ring-opening polymerization. The triblock copolymers were then subjected to stereocomplexation of the enantiomeric blocks followed by acidic hydrolysis of the amorphous racemic blocks to obtain uniform in size stereocomplex nanocrystals (scNCs) consisting only of near-perfect stereocomplex. Hydrolysis conditions were optimized based on DSC analyses and scNCs crystal structure was confirmed by XRD. The morphology of sc-b-P(rac-LA)-b-sc and scNCs was studied by peak-force tapping atomic force microscopy, allowing simultaneous topography and adhesion mapping image analyses. The results clearly evidenced the recovery of narrowly dispersed low-adhesive mostly spherical nanoparticles with average diameter of 15±4 nm with concentration-controlled shape and size. Such unprecedented all-PLA stereocomplexed nanocrystals might find applications as renewable nanofillers in all-PLA nanocomposites.

Introduction

Nowadays, environmental and sustainability concerns are focusing towards the implementation of polymers from renewable resources for materials and/or energy applications.[1] Amongst all, poly(lactic acid) (PLA)-based materials related with their property of biodegradation have been intensively developed for short-time applications going from drug-carriers and implants to packaging and textiles.[2] More recently, PLA-based materials have found higher added value (durable) applications in automotive, communication and electronic industries, e.g. as "green" notebooks, cell phones[3] and panels for DVD drivers.[4] However, due to the relatively limited thermo-mechanical properties of this aliphatic polyester, PLA-based materials may require the use of nano-sized reinforcements.[5;6]

The small size of the nano-reinforcing agents (nanoparticles, nanofillers) provides a very large surface/volume ratio expected to dramatically improve thermal and mechanical properties, and processing characteristics of the resulting polymeric nanocomposite material.[7] In general, a content in the range of 3 to max. 10 wt% is needed for reaching satisfactory properties while most often conventional (micro)composites do require much higher quantity in microfillers, which can even exceed 60 wt%.[8] However, one of the most difficulties to attain such level of performance relies on the possibility to distribute and disperse the nanoparticles as finely as possible throughout the polymer matrix, ideally resulting in strong nanofiller-polymer interfacial interactions.[9] Different strategies, mostly involving either physical or chemical surface modification of the nanofillers have been developed to improve the interfacial compatibility between the polymer matrix and nanoparticles.[10-15] Although positive outcomes and uses are somehow achieved in the literature, a considerable attention is focused on the development of all-the same component-composites (where both the matrix and nanofiller are of the same chemical composition),[16] thus overcoming the inherent incompatibility of the nanofiller and the polymer matrix and their potential recyclability.

The strategy for all-the same component-composites was initially proposed by Matsumura et al.[17] in the preparation of all-cellulose nanocomposites of improved mechanical properties and of recycling potential. The first stage involved the preparation of uniform cellulosic nanoparticles (nanocrystals), combining high surface area, low density, and good mechanical properties with high flexural strength and high stiffness.[18,19] Usually, cellulose nanocrystals are obtained via acidic hydrolysis of the non-crystalline (amorphous) and the

para-crystalline regions of cellulose fibers,[20] while the crystalline fraction remains unchanged. As a result, rod-like cellulose nanoparticles of almost perfect crystal structure and uniform size distribution are obtained.

The design of crystalline PLA nanoparticles with enhanced thermal and mechanical stability can be readily obtained through stereocomplexation of both PLA of D- and L-configuration. An interesting strategy to obtain monodisperse PLA-based nanoparticles is exploited by Kang et al.[21] who have prepared stable narrowly dispersed PLA nanoparticles via stereocomplexation. Stereocomplexation consists in exclusive racemic crystallization when enantiomeric L- and D-lactide units coexist in a system.[22,23] The process results in a shift of PLA melting temperature from 170–180 °C to 210- 230 °C and largely improves the thermo-mechanical properties of the stereocomplexed material with respect to pure enantiomeric PLA. Unfortunately the preparation of such nanoparticles involves the use of amphiphilic copolymers[24-28] or hybrid nanoparticles,[29] largely deviating from the all-PLA nanomaterials concept.

Hence, the present study aims at the preparation of uniform in shape and size PLA nanocrystals. A two-step approach, consisting in solution stereocomplexation of enantiomeric PLA sequences, separated by a central amorphous P(rac-LA) block in all-PLA symmetric triblock copolymers followed by acid hydrolysis of the amorphous blocks is proposed. Their crystallinity and structure were monitored by differential scanning calorimetry (DSC), X-ray diffraction (XRD) and Peak Force Tapping Atomic Force Microscopy (PFT-AFM). The following results are unprecedented and offer uniform in size and shape all-PLA stereocomplexed nanocrystals as attractive nanofillers for all-PLA nanocomposites.

Experimental

Methods

Synthesis of α,ω-OH P(rac-LA). The reaction was performed in a 500 ml round-bottom glass reactor equipped with a nitrogen inlet, cooling system, and mechanical stirrer. For the synthesis, 150 g rac-LA (1.04 mol, 28 eq.) were charged in the reactor and stirred at 160 °C under nitrogen until the complete melting of monomer. Then, 3.3 ml (3.35 g, 37.2 mmol, 1 eq.) BDO followed by 5.6 ml of Sn(Oct)$_2$/Ph$_3$P (1:1 molar ratio, 3.7×10^{-2} mol/L) solution in dry toluene were added via a syringe at an initial $[LA]_0$-to-$[Sn(Oct)_2]_0$ molar ratio of 5,000. The polymerization was performed under gentle stirring (50 rpm) in inert atmosphere at 160 °C for 30 min. The viscous reaction medium was then transferred to an aluminum bark and let to cool down to room temperature (r.t.). For purification, the polymer was dissolved in chloroform and washed once with 0.1 M aqueous hydrochloric acid solution, then twice with demineralized water for catalyst extraction, and precipitated in 7-fold (v/v) excess of cold heptane. The white precipitate was recovered by filtering and drying to constant weight at 40 °C under reduced pressure overnight.

Synthesis of P(D,D(L,L)-LA)-b-P(rac-LA)-b-P(D,D(L,L)-LA). The α,ω-OH P(rac-LA)-initiated ROP of D,D(L,L)-LA was performed in a flame-dried 250 ml round-bottom flask equipped with a magnetic stirrer and a three-way rubber-septum-capped stopcock. About 10 g (6.9×10^{-2} mol, 70 eq) D,D(L,L)-LA were charged into the flask using the inert atmosphere of the glove box. Then, 50 ml dry toluene were added via a flame-dried syringe

equipped with a stainless steel capillary under N$_2$. The flask was placed into an oil bath set at 70°C and after complete D,D(L,L)-LA dissolution 0.37 ml of Sn(Oct)$_2$/Ph$_3$P (1:1 molar ratio, 3.7×10^{-2} mol/L) solution in dry toluene were added via a syringe for a $[LA]_0$/$[Sn(Oct)_2]_0$ molar ratio of 5,000. 4.17 g (9.93×10^{-4} mol, 1 eq) P(rac-LA) were simultaneously dissolved at 70°C in 20 ml dry toluene and transferred to the D,D(L,L)-LA solution ([LA] = 1 mol). For kinetic studies, aliquots were taken at predetermined time intervals (4, 24, 48 and 72 h) and directly precipitated in 7-fold excess of cold heptane (v/v). The obtained products were dried under vacuum to a constant weight at 25 °C to remove heptane and then at 80°C to remove unreacted monomer. For the synthesis of P(D,D-LA)-b-P(rac-LA)-b-P(D,D-LA) and P(L,L-LA)-b-P(rac-LA)-b-P(L,L-LA) samples, the α,ω-dihydroxyl P(rac-LA)-initiated ROP of D,D(L,L)-LA started without any initiator purification and was allowed to run at 70°C for 72 h. The viscous reaction medium was then let to cool down to room temperature (r.t.), the solvent was evaporated under reduced pressure and product purification followed the procedure described in the previous section.

Stereocomplexation. Stereocomplexation of P(D,D-LA)-b-P(rac-LA)-b-P(D,D-LA) and P(L,L-LA)-b-P(rac-LA)-b-P(L,L-LA) was performed following a previously described procedure [30]. At first the triblock enantiomeric copolymers were separately dissolved in CHCl$_3$ (1 g/dL) to obtain clear solutions. At second, the clear solutions were mixed at a molar ratio of [L,L-LA]-to-[D,D-LA] = 1:1 for 3 h. Finally, the solvent was evaporated at r.t., and the obtained powders were dried at 60 ° C under reduced pressure up to constant weight.

Hydrolysis. A pre-weighed amount (0.1 g) of stereocomplex was charged in a round-bottom flask equipped with a magnetic stirrer and a three-way stop-cock sealed with a rubber septum. 11.4 ml of dry toluene were then added and the flask was transferred to an oil bath preheated at 80 °C. After 10 min homogeneous dispersion of stereocomplex was achieved and 1 ml of conc. HCl (37 %) was added via a syringe. Keeping temperature unchanged, hydrolysis got continued under stirring at 250 rpm for 50h. Samples were taken at predetermined time intervals (1, 3, 4, 6, 7, 8, 24, 26, 40, 48 and 50h), precipitated in cold methanol overnight, centrifuged at 4,000 rpm for 30 min for supernatant removal and dried under reduced pressure to constant weight at 60 °C. After the optimal conditions were settled down hydrolysis was performed on high amount of stereocomplex (6 g) for 6h. The solvent and HCl amounts were consequently recalculated for up-scaling. As-hydrolyzed materials were then recovered as described above.

Dispersion in chloroform. Dispersions of the non-hydrolyzed and the hydrolyzed stereocomplexes (0.5 mg/ml or 8 mg/ml in CHCl$_3$) were obtained by sonication for 2 min.

Results and discussion

Synthesis and characterization of P(D,D(L,L)-LA)-b-P(rac-LA)-b-P(D,D(L,L)-LA) triblock enantiomeric copolymer

Two enantiomeric P(D,D-LA)-b-P(rac-LA)-b-P(D,D-LA) and P(L,L-LA)-b-P(rac-LA)-b-P(L,L-LA) triblock copolymers were first obtained using a two-step ring-opening polymerization (ROP) (Scheme 1).

Journal of Materials Chemistry A

ARTICLE
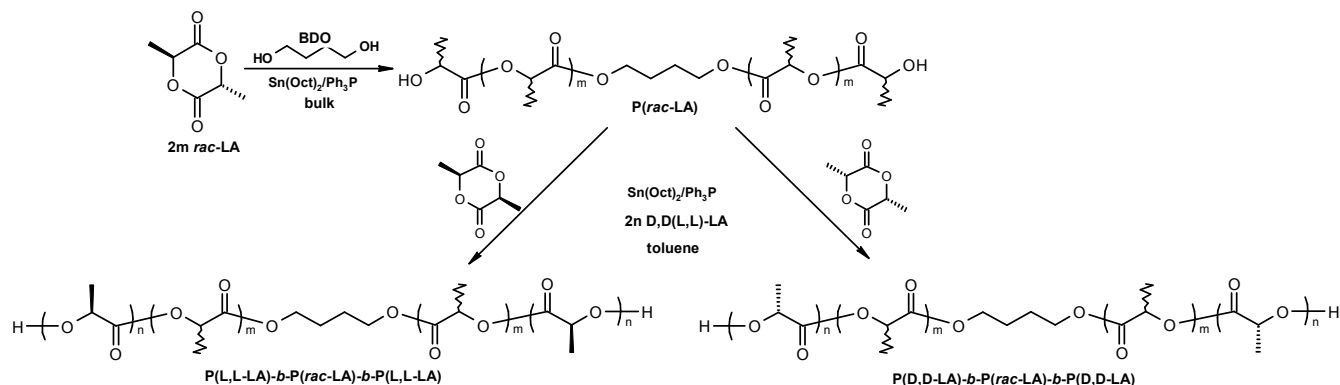
Scheme 1. Synthetic pathway to enantiomeric copolymers (m = n)

At first ROP of *rac*-lactide (*rac*-LA) was performed in bulk using $Sn(Oct)_2/Ph_3P$ as catalyst and BDO as initiator. Afterwards, an α,ω-dihydroxyl P(*rac*-LA) macroinitiator was obtained and used (after purification) in the respective ROP of enantiomeric D,D- or L,L-LA performed in toluene again using $Sn(Oct)_2/Ph_3P$ as catalyst. To achieve an optimal stereocomplexation of enantiomeric PDLA and PLLA-based chains,[22,23] the targeted $\overline{M}_n$ of both P(D,D-LA) and P(L,L-LA) blocks was kept low, *i.e.*, 5000 g/mol. Then, the optimal conditions for the L,L-LA ROP were determined based on kinetic studies (Table 1, Figure 1).
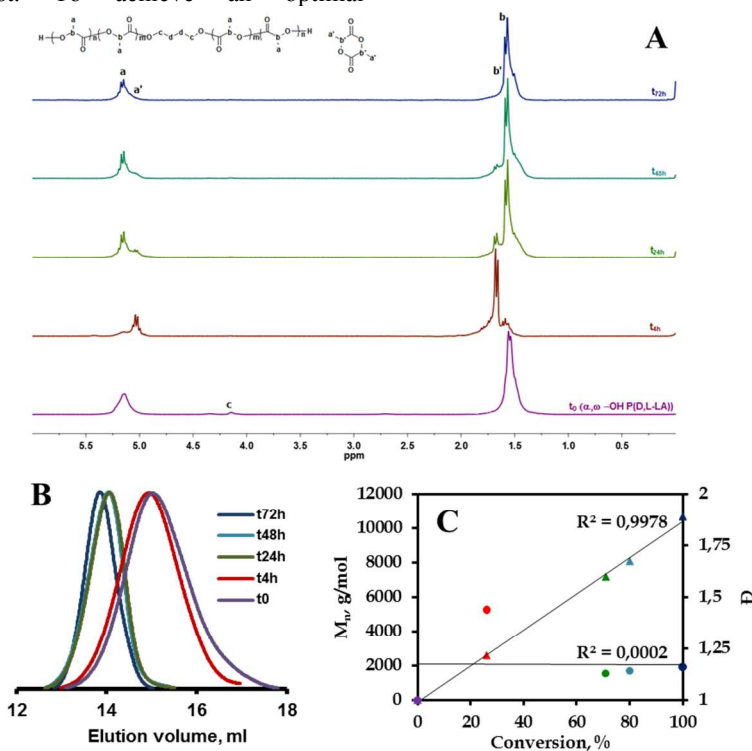
Figure 1. ^{1}H NMR spectra (A), SEC elugrams (B), and evolution of $\overline{M}_n$ (▲) and Đ (●) *vs.* conversion (C) for the α,ω-dihydroxyl P(*rac*-LA)-initiated ROP of L,L-LA (Entries 1-5, Table 1)

Table 1. Molecular characteristics of the enantiomeric P(D,D-LA)-*b*-P(*rac*-LA)-*b*-P(D,D-LA) and P(L,L-LA)-*b*-P(*rac*-LA)-*b*-P(L,L-LA) triblock copolymers. For comparison, the characteristics of the starting macroinitiator are also given.

Entry	Composition	t, h	Yield, %[a]	NMR			SEC		
				Conversion, %	DP	$\overline{M}_n^b$	$\overline{M}_n^{PS}$	$\overline{M}_W^{PS}$	Đ
1	α,ω-OH P(*rac*-LA)	0	98	100	41	6,000	6,800	12,200	1.63
2		4	20	26	18	2,600	9,000	13,000	1.44
3	P(L,L-LA)-*b*-P(*rac*-LA)-*b*-P(L,L-LA)	24	83	71	50	7,200	24,800	28,200	1.13
4		48	89	80	56	8,100	25,400	28,900	1.14
5		72	96	≈100	70	10,100	25,300	29,300	1.16
6		72	97	≈100	70	10,100	23,200	25,600	1.10
7	P(D,D-LA)-*b*-P(*rac*-LA)-*b*-P(D,D-LA)	72	98	≈100	70	10,100	24,000	26,600	1.11

[a] Determined by gravimetry. [b] Calculated with correction for the presence of the macroinitiator.

All raw samples were characterized by ^{1}H NMR and SEC techniques. The spectroscopic analyses clearly indicated the progressive monomer consumption with time and the full conversion was reached within 72 h (Figure 1A). This was in agreement with SEC analyses, showing up the shift of the peak to lower elution volumes (Figure 1B) with time and confirming the increase in molar mass. Moreover, the plot of the $\overline{M}_n$ and the dispersity (Đ) *vs.* conversion (Figure 1C) is linear, highlighting a good control over the chain-growth polymerization under the prevailing conditions. The good control over the molecular parameters of the enantiomeric P(D,D-LA)-*b*-P(*rac*-LA)-*b*-P(D,D-LA) and P(L,L-LA)-*b*-P(*rac*-LA)-*b*-P(L,L-LA) triblock copolymers was again confirmed in a "one-pot" synthetic procedure whose two enantiomeric P(D,D-LA)-*b*-P(*rac*-LA)-*b*-P(D,D-LA) and P(L,L-LA)-*b*-P(*rac*-LA)-*b*-P(L,L-LA) triblock copolymers of $\overline{M}_n$ = 10,100 g/mol and Đ = 1.10-1.11 were obtained after consecutive polymerization of *rac*-LA and LA of D- or L-configuration (Entries 6 and 7, Table 1).

Preparation and characterization of scNCs

The stereocomplex nanocrystals (scNCs) were obtained applying a two-step procedure involving first the stereocomplexation of both enantiomeric triblock copolymer partners and then the hydrolysis of the amorphous P(*rac*-LA) middle blocks. Stoichiometric amounts of P(D,D-LA)- and P(L,L-LA)-block were used and the formation of stereocomplex was confirmed by DSC. The results are shown in Figure 2. For comparison, the DSC thermograms of the α,ω-dihydroxyl P(*rac*-LA) macroinitiator and the P(D,D-LA)-*b*-P(*rac*-LA)-*b*-P(D,D-LA), P(L,L-LA)-*b*-P(*rac*-LA)-*b*-P(L,L-LA) are also given. In all cases first heating run was carried out to erase the sample thermal history and only data from the second heating runs were used. As might be seen, a T_g for all materials was clearly visible upon heating and lies in the range of 40 to 50 °C. In agreement with its *racemic* nature, the macroinitiator did not show any cold crystallization or melting, while cold crystallization (T_{cc}) occurred upon the second heating scan of the enantiomeric triblock copolymers. This cold crystallization overlaps the crystal melting, impeding the correct calculations of the corresponding enthalpies (of cold crystallization (ΔH_{cc}) and melting (ΔH_m)). However, both triblock copolymers could be considered nearly amorphous as values of less than 1 (0.6961 J/g for ΔH_m of P(L,L-LA)-*b*-P(*rac*-LA)-*b*-P(L,L-LA) and 0.6431 J/g for ΔH_m of P(D,D-LA)-*b*-P(*rac*-LA)-*b*-P(D,D-LA)) were calculated after subtracting ΔH_{cc} from ΔH_m. Interestingly, both

enantiomeric copolymers showed multiple meltings, that might be attributed to the presence of crystals of different size and/or perfection, and/or their reorganization and transition from one structure to another depending on the DSC cooling/heating rate.[35]
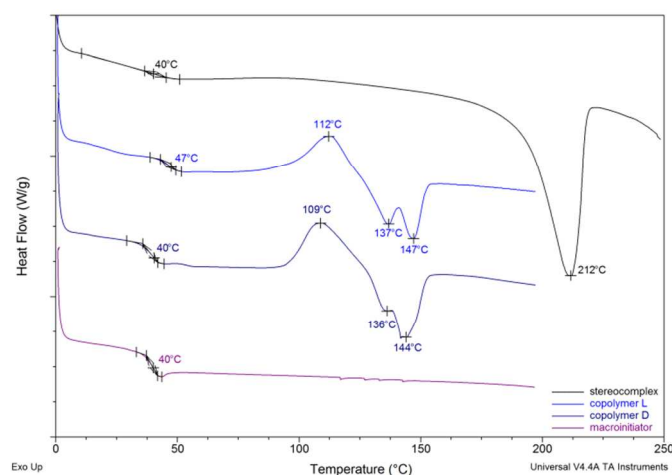
Figure 2. DSC thermograms recorded during the second heating run

The DSC thermogram of the stereocomplexed sample (sc-*b*-P(*rac*-LA)-*b*-sc) features interesting differences. For instance no visible T_{cc} is noticed on the second heating scan. This suggests highly improved crystallinity and crystallization rate as expected for stereocomplexed materials. In agreement, a single melting endotherm at 212°C (ΔH_m = 64.20 J/g) was recorded.[22,23] Indeed, the T_m of starting triblock copolymers is shifted to much higher temperature (212 °C), e.g. an increase by about 65-70 °C. The high crystallinity of the stereocomplexed materials limits the accuracy of T_g measurement but it might be supposed to appear at about 40 °C in agreement with the values determined for the separate copolymers. Both triblock copolymers present similar heat capacity changes (Δc_p = 0.46-0.47 J/g·°C), while the value calculated for the stereocomplexed sample was rather law (Δc_p = 0.2626 J/g·°C) as expected for highly crystalline samples. It might be concluded that the presence of the amorphous P(*rac*-LA)-block does not prevent the stereocomplexation of P(D,D-LA) and P(L,L-LA) sequences. Similar observations were reported for other enantiomeric lactide containing block copolymers.[25,36]

Subsequently, the obtained stereocomplex was subjected to acidic hydrolysis of the P(*rac*-LA) middle block. The idea was

inspired from the recovery of cellulose nanocrystals of near-perfect crystalline structure.[37] It was supposed that the acidic hydrolysis, when performed in a bad solvent medium (a non-solvent for PLA), will preferentially affect the amorphous regions of the sc-*b*-P(*rac*-LA)-*b*-sc sample as they are more susceptible to swelling and attack than the crystalline domains. In other terms, uniform in size nanoparticles consisting only of near-perfect stereocomplexes were expected to be generated.

The acidic hydrolysis of sc-*b*-P(*rac*-LA)-*b*-sc was studied in the presence of concentrated hydrochloric acid for predetermined time intervals of up to 50 h (Table 2, Figure 3).
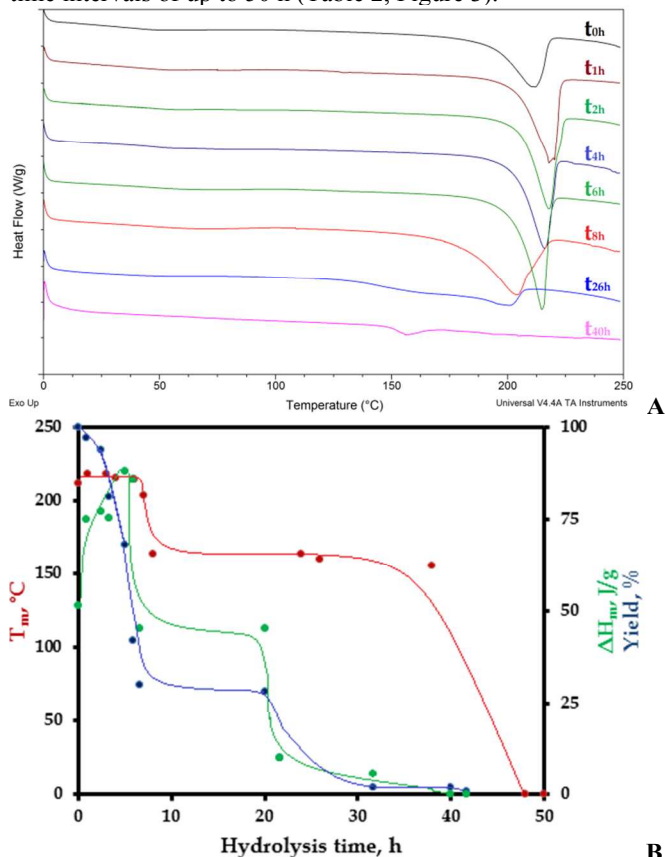
Figure 3. Selected DSC thermograms (A) and dependence of T_m, ΔH_m and recovery yield (B) on hydrolysis time

The recovery yield, visual aspect, T_m and melting enthalpy ΔH_m (first heating run) of the settled samples were followed as parameters for the completion of reaction. As might be seen from Table 2, recovery yield continuously decreased with hydrolysis time from 97 to 1 % and reached 68 % after 6 h. This yield was very close to the theoretical calculations assuming that the entire amorphous part is hydrolyzed (66 %) and suggests that predominantly pure highly crystalline sc particles were recovered. In agreement, the values of ΔH_m initially increased from 51.28 J/g (before hydrolysis) to 88.20

J/g (after 6 h of hydrolysis) and further continuously decreased with hydrolysis time. Concerning the T_m, it remained insignificantly changed up to 6 h of hydrolysis and followed the yield and ΔH_m dependences, resulting in nearly amorphous material after 48 h of reaction. Such a behavior was already observed for other semi-crystalline materials where at first the amorphous part gets predominantly hydrolyzed until its complete disappearance and followed by the hydrolysis of the crystalline part of the material.[38] Based on a comparative analysis of all three parameters (Figure 3B) the optimal hydrolysis conditions were determined to lay between 5 and 6 h of hydrolysis.

Table 2. Recovery yield, aspect and thermal characteristics (DSC) of sc-*b*-P(*rac*-LA)-*b*-sc vs hydrolysis time.

| Entry | Hydrolysis time, h | Recovery yield, % | Visual aspect | DSC | |
				T_m, °C	ΔH_m, J/g
1	0	100		212	51.28
2	1	97		218	74.84
3	3	94		218	77.36
4	4	81	Solid	216	77.35
5	6	68		215	88.20
6	7	42		204	85.87
7	8	30		164	45.35
8	24	28	Waxy solid		
9	26	10		160	10.15
10	40	2		156	5.45
11	48	2	Viscous liquid	no	0
12	50	1		no	0

As seen and in agreement with the literature,[39] the P(L,L-LA)-*b*-P(*rac*-LA)-*b*-P(L,L-LA) pattern (Figure 4A) presented diffraction peaks at $2\theta = 14.8°$, 16.7°, 19.1°, 22.4°, 28.9° distinctive for the α-form of optically pure P(L,L(D,D)-LA) crystallizing in a pseudo-orthorhombic unit cell of $l0_3$ helices. In sc-*b*-P(*rac*-LA)-*b*-sc (Figure 4B) these peaks vanished and new diffraction peaks were observed at $2\theta = 11.9°$, 20.7°, and 24.0°, attributed to the triclinic crystals of stereocomplexed P(L,L-LA)/P(D,D-LA) blocks of 3_1 helices.[22,23] This confirms the absence of P(L,L-LA)-*b*-P(*rac*-LA)-*b*-P(L,L-LA) homocrystallites after complete stereocomplexation. Similar crystal structure can be reasonably ascribed to the scNCs after 6h of acidic hydrolysis (Figure 4C). Essentially, in comparison to the starting sc-*b*-P(*rac*-LA)-*b*-sc, scNCs showed a decreased amorphous pattern, confirming the predominant hydrolysis of the amorphous P(*rac*-LA) middle blocks. Interestingly enough, the morphology of sc-*b*-P(*rac*-LA)-*b*-sc and scNCs was further studied by Peak Force Tapping Atom Force Microscopy (PFT-AFM).

Journal of Materials Chemistry A

ARTICLE
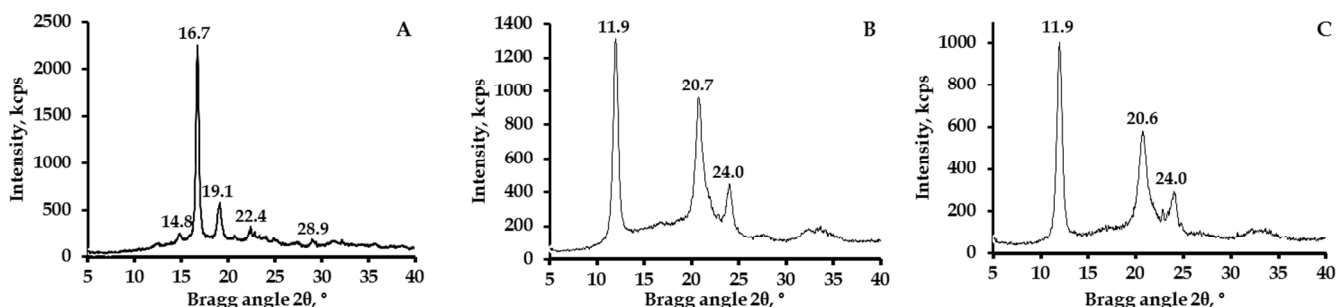
Figure 4. XRD patterns of: A) the P(L,L-LA)-*b*-P(*rac*-LA)-*b*-P(L,L-LA), B) the sc-*b*-P(*rac*-LA)-*b*-sc, C) the scNCs (after 6h of hydrolysis, see Table 2)

The PFT-AFM is a recent oscillating-probe AFM technique, simultaneously visualizing the sample topography (i.e., the surface morphology) and providing quantitative information on the surface mechanical properties (adhesion, Young's modulus, deformation or dissipation).[32,34] It also allows better understanding of the height images. The topography and the adhesion mapping (the minima of the force distance curve) images of sc-*b*-P(*rac*-LA)-*b*-sc and scNCs (recovered after 6 h of hydrolysis) are shown in Figure 5. Samples were prepared by dispersing dried sc-containing particles in chloroform at different concentration and deposition of 1 µl dispersion on *i*-propanol cleaned individual glass-slides. As might be seen, the topographic PFT-AFM imaging of sc-*b*-P(*rac*-LA)-*b*-sc before hydrolysis shows the formation of round-to-oblong objects with wide diameter distribution ranging from 20±5 nm to 190±9 nm (Figure 5A). Adhesion mapping confirmed the topography observations and revealed low-adhesion profile of the visualized entities compared to the matrix (Figure 5B). Intriguingly, a closer look presented a gradient of adhesion related with two low-adhesion zones, which are separated by a layer of higher adhesion. Knowing that the mechanical properties are often affected by the topographic features, and taking the deformation data into account, it might be concluded that this adhesion mapping gradient is mainly due to the chemical nature of the studied material. Therefore, and considering the sc-*b*-P(*rac*-LA)-*b*-sc inherent structure, one can extrapolate the low-adhesion zones to sc parts and the higher adhesion layer to the amorphous P(*rac*-LA) blocks. Additionally, Young's modulus estimation was performed using the Derjaguin-Müller-Toporov (DMT) method after an appropriate tip calibration[32] providing values of 100±30 MPa.
Hydrolysis clearly changed the morphology of these materials, as shown in Figure 5C and D. The number and the size of the big aggregates were both found to decrease, leading to narrowly dispersed mostly spherical particles with average diameter of 15±4 nm. Their identification and characterization (in terms of size and shape) was difficult based only on the height images and was done by comparing analyses with adhesion images, where the particles appeared as entities of very low adhesion (Figure 5D). These results, together with the DSC and XRD data somehow confirmed the extrapolation of the low-adhesion zones to sc parts and the higher adhesion layer to the

amorphous P(*rac*-LA) blocks in the case of sc-*b*-P(*rac*-LA)-*b*-sc.
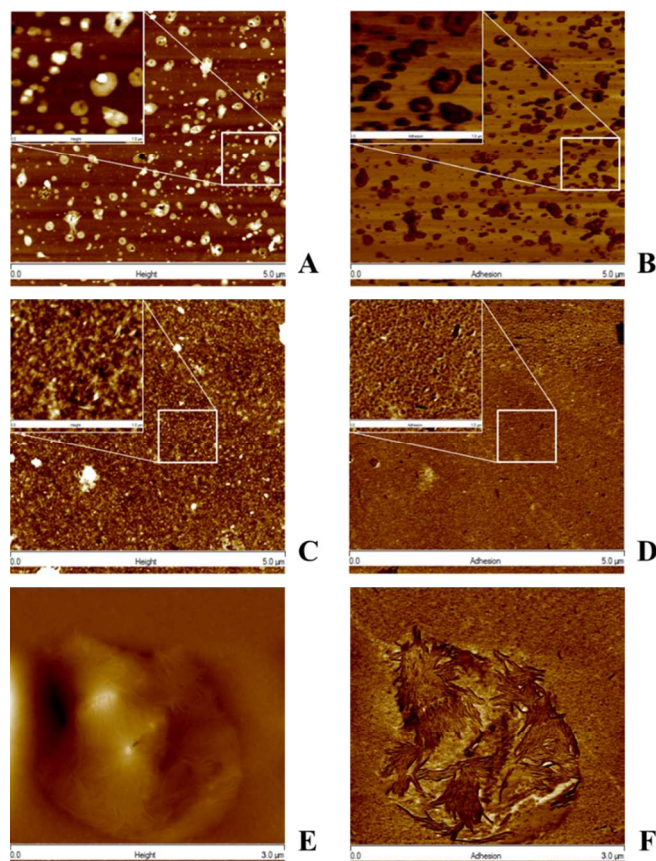
Figure 5. PFT-AFM topographic (A, C and D) and adhesion mapping (B, D and F) images of sc-*b*-P(*rac*-LA)-*b*-sc (A and B) and scNCs (recovered after 6h of hydrolysis, C-F) as obtained by casting of chloroform dispersions of 0.5 mg/ml (A-D) and 8 mg/ml (E and F). Magnification at 1 × 1 µm is given at the upper left corner of images A-D. The scan size is 5 × 5 µm for images A-D and 3 × 3 µm for E and F.

Surprisingly, cylindrical non-adhesive formations with average width of ca. 15±2 nm and average length of ca. 130±20 nm were also seen. Taking into account the molecular characteristics of the initial triblock-copolymers, their presence might be ascribed to secondary aggregation of the spherical particles as observed in other systems.[39,40] As cylindrical aggregates formation is strongly dependent on particle concentration,[39,40] samples for AFM observations were prepared from chloroform dispersions of the scNCs at 8 mg/ml (Figure 5E and F). In agreement with the here proposed concentration dependent secondary aggregation of the scNCs, cylindrical structures were found to form large aggregates, dispersed in a matrix of small spherical particles. The Young's modulus estimations revealed values of 100±20 MPa and of 150±25 MPa for the spherical and for the cylindrical non-adhesive nanocrystals, respectively. This may bring to the conclusion that the modulus was only slightly influenced by the particle shape. However, the values should only be considered as approximate as they were found to depend upon particle size and distribution as well as on the film thickness. Such concentration dependent aggregation behavior might be useful in some potential applications of the scNCs. Further studies on the application of the all-PLA stereocomplexed nanocrystals as nanofillers for all-PLA nanomaterials are currently under progress.

Conclusions

Enantiomeric P(D,D-LA)-b-P(rac-LA)-b-P(D,D-LA) and P(L,L-LA)-b-P(rac-LA)-b-P(L,L-LA) triblock copolymers were synthesized applying a two-step ring-opening polymerization. At first, ROP of rac-LA was performed in bulk to obtain an α,ω-dihydroxyl P(rac-LA). This product was next used as a macroinitiator in the solution ROP of D,D- or L,L-LA. The optimal conditions for the lactide ROP were determined based on kinetic studies indicating linear dependence of the number-average molar mass vs. conversion up to full monomer conversion within 72 h. Finally, a "one-pot" synthetic process leading to P(D,D-LA)-b-P(rac-LA)-b-P(D,D-LA) and P(L,L-LA)-b-P(rac-LA)-b-P(L,L-LA) of $\overline{M}_n$ = 10,100 g/mol and Đ = 1.10-1.11 was successfully developed. The as-obtained P(D,D-LA)-b-P(rac-LA)-b-P(D,D-LA) and P(L,L-LA)-b-P(rac-LA)-b-P(L,L-LA) were stereocomplexed from diluted (1 mg/ml) chloroform solutions at stoichiometric conditions, and further hydrolyzed to obtain scNCs. Hydrolysis conditions were optimized based on DSC analyses and scNCs crystal structure was confirmed by XRD.

The morphology of sc-b-P(rac-LA)-b-sc and scNCs was then studied by PFT-AFM. Simultaneous topography and adhesion mapping images analyses of sc-b-P(rac-LA)-b-sc showed adhesion gradient forming two low-adhesion zones separated by a layer of higher adhesion extrapolated the sc parts and the amorphous P(rac-LA) blocks, respectively. In contrast, hydrolysis clearly left place to narrowly dispersed mostly spherical low-adhesive particles with average diameter of 15±4 nm. Their presence was accompanied by cylindrical non-adhesive formations with average width of ca. 15±2 nm and average length of ca. 130±20 nm ascribed to secondary aggregation. Such unprecedented all-PLA stereocomplexed nanocrystals are attractive nanofillers for all-PLA nanomaterials.

Notes and references

[a] Laboratory of Polymeric and Composite Materials, Center of Innovation and Research in Materials and Polymers (CIRMAP), University of Mons (UMONS), Place du Parc 20, 7000 Mons, Belgium. Correspondence to: philippe.dubois@umons.ac.be

[b] Laboratory for Chemistry of Novel Materials (CMN), Center of Innovation and Research in Materials and Polymers (CIRMAP), University of Mons, Place du Parc 23, B-7000 Mons, Belgium.

[c] Department of Advanced Materials and Structures (AMS), Centre de Recherche Public Henri Tudor, Rue Bommel 5, 4940 Hautcharage, Luxembourg.

Materials. rac-Lactide (rac-LA, Purasorb® D,L), L,L-lactide (L,L-LA, Purasorb® L) and D,D-lactide (D,D-LA, Purasorb® D) with optical purity > 99.5% (MW = 144 g/mol, free acid < 1 meq/kg, water content < 0.02%) were supplied by Purac Biochem BV (the Netherlands) and stored in a glove box prior to use. Triphenylphosphine (Ph$_3$P, MW = 262 g/mol, ≥ 99 %, Merck) was recrystallized from diethylether, dried at 25 °C under reduced pressure overnight and then by three consecutive azeotropic distillations with dry toluene prior to use. Toluene (Labscan, 99%) was dried using an MBraun solvent purification system under N2 flow. 1,4-Butanediol (BDO, MW = 90 g/mol, > 98 %, Kosher) and stannous octoate (Sn(Oct)$_2$, MW = 405.01 g/mol, ~95 %, Aldrich) were used as received. Chloroform (Chem-Laboratory, 99.8%), heptane (Labscan, 99%), methanol (Chem-Laboratory, 99.8%), toluene (Acros, 99%), hydrochloric acid (Emsure, 37 %) and all other reagents were analytical reagent (AR) grade and used as received.

Characterization. ^{1}H NMR spectra were recorded on a Bruker 500 MHz spectrometer using deuterated chloroform (CDCl$_3$) as solvent and tetramethylsilane (TMS) as internal reference. The concentration of sample solution was about 30 mg/mL or less.

Size exclusion chromatography (SEC) was performed in CHCl$_3$ at 30 °C using an Agilent liquid chromatograph equipped with an Agilent degasser, an isocratic HPLC pump (flow rate = 1 mL/min), an Agilent autosampler (loop volume = 200 μL, solution conc. = 2 mg/mL), an Agilent-DRI refractive index detector and three columns: a PL gel 10 μm guard column and two PL gel Mixed-D 10 μm columns (linear columns for separation of PS ranging from 500 to 106 g/mol). Polystyrene standards were used for calibration.

Differential scanning calorimetry (DSC) was performed on a DSC Q2000 apparatus from T.A. Instruments under nitrogen flow (heating rate 10 °C/min). For non-isothermal experiments, a heat/cool/heat procedure was used starting from 0 °C and going up to 200 °C (first heating) and 250 °C (second heating). First heating run was considered to erase thermal history of all samples and to permit evaluation of the role of the stereocomplex (sc) onto HMPLA crystallization. Thus, melt crystallization

(T_c) and enthalpy of melt crystallization (ΔH_c) were obtained from the first cooling run. Glass transition (T_g), cold crystallization (T_{cc}), and melting (T_m) temperatures (and their corresponding enthalpies (ΔH)) were acquired from the second heating run.

X-ray diffraction (XRD) morphological analyses were performed on a Siemens D5000 diffractometer using Cu-KR radiation (wavelength: 1.5406 Å) at room temperature. The samples were step-scanned from 10 ° to 25 ° in 2 θ with steps of 0.02 ° with fi xed counting time of 4 s (40 kV, 30 mA).

Peak Force Tapping Atomic Force Microscopy (PFT-AFM) was performed on samples with concentrations of 0.5 mg/ml to 8.0 mg/ml using a Dimension Icon (Bruker Nano Inc, Santa Barbara (SB), CA, USA) AFM driven by a Nanoscope V control unit.[31,32,34] The microscope operated in air, at room temperature and at atmospheric pressure; using a sharp silicon nitride probe (SNL, Bruker, SB, CA, USA) with a spring constant (k) of 0.35 N/m. The force distance curves were recorded at operating frequency of 2 kHz. The size of the observed particles was determined using the Direct Measurements on Single Particles method (using the ImageJ software) for at least 100 particles from at least 3 different AFM images of 5 μm × 5 μm. The samples of different concentration were obtained using the dilution method. Prior to analyses, drops of 1 μl were deposited on i-propanol-cleaned glass-slides and air-dried.

1 J. A. Dahl, B. L. S. Maddux and J. E. Hutchinson, *Chem. Rev.*, 2007, **107**, 2228.

2 J.-M. Raquez, R. Mincheva, O. Coulembier and Ph. Dubois, In: K. Matyjaszewski and M. Möller (eds.) *Polymer Science: A Comprehensive Reference*, 2012, **4**, 761.

3 M. Darder, P. Aranda and E. Ruiz-Hitzky, *Adv. Mater.*, 2000, **19**, 1309.

4 O. Muench, *Bioplastics Magazine*, 2008, **3**, 10.

5 M. Alexandre and Ph. Dubois, *Mater. Sci. Eng. R. Rep.*, 2000, **28**, 1.

6 P. Bordes, E. Pollet and L. Avérous, *Prog. Polym. Sci.*, 2009, **34**, 125.

7 H. Liu and L. C. Brinson, *Trans. ASME*, 2006, **73**, 758.

8 L. E. Nielsen and R. F. Landel, *Mechanical Properties of Polymers and Composites. 2nd edition*, New York, Marcel Dekker, Inc., 1994, 377.

9 P. Akcora, H. Liu, S. K. Kumar, J. Moll, Y. Li, B. C. Benicewicz, L. S. Schadler, D. Acehan, A. Z. Panagiotopoulos, V. Pryamitsyn, V. Ganesan, J. Ilavsky, P. Thiyagarajan, R. H. Colby and J. F. Douglas, *Nature Mater.*, 2009, **8**, 354.

10 K. Oksman, A. P. Mathew, D. Bondeson and I. Kvien, *Comp. Sci. Technol.*, 2006, **66**, 2776.

11 D. Bondeson and K. Oksman, *Composites A,* 2007, **38**, 2486.

12 D. Bondeson and K. Oksman, *Compos. Interf.*, 2007, **14**, 617.

13 N. Lin, J. Huang, P. R. Chang, J. Feng and J. Yu, *Carbohyd. Polym.*, 2011, **83**, 1834.

14 A. Pei, Q. Zhou and L. A. Berglund, *Composites Sci. Technol.*, 2010, **70**, 815.

15 A.-L. Goffin, J.-M. Raquez, E. Duquesne, G. Siqueira, Y. Habibi, A. Dufresne and P. Dubois, *Biomacromolecules*, 2011, **12**, 2456.

16 J.-M. Raquez, Y. Habibi, M. Murariu and P. Dubois, *Prog. Polym. Sci.*, 2013, **38**, 1504.

17 H. Matsumura, J. Sugiyama and W. G. Glasser, *J. Appl. Polym. Sci.*, 2000, **78**, 2242.

18 A. Šturcová, G. R. Davies and S. J. Eichhom, *Biomacromolecules*, 2005, **6**, 1055.

19 X. Cao, H. Dong and C. M. Li, *Biomacromolecules*, 2007, **8**, 899.

20 J. Araki, M. Wada, S. Kuga and T. Okano, *Colloids Surf. A*, 1998, **142**, 75.

21 N. Kang, M.-È. Perron, R. E. Prud'homme, Y. Zhang, G. Gaucher and J.-C. Leroux, *Nano Lett.*, 2005, **5**, 315.

22 H. Tsuji, S.-H. Hyon and Y. Ikada, *Macromolecules*, 1991, **24**, 5657.

23 H. Tsuji, F. Horii, M. Nakagawa, Y. Ikada, H. Odami and K. Kitamaru, *Macromolecules*, 1992, **25**, 4114.

24 T. Fujiwara, T. Mukose, T. Yamaoka, H. Yamane, S. Sakurai and Y. Kimura, *Macromol. Biosci.*, 2001, **1**, 204.

25 K. Fukushima, R. C. Pratt, F. Nederberg, J. P. K. Tan, Y. Y. Yang, R. M. Waymouth and J. L. Hedrick, *Biomacromolecules*, 2008, **9**, 3051.

26 X. D. Guo, J. P. K. Tan, S. H. Kim, L. J. Zhang, Y. Zhang, J. L. Hedrick, Y. Y. Yang and Y. Qian, *Biomaterials*, 2009, **30**, 6556.

27 N. Kang, M. E. Perron, R. E. Prud'homme, Y. B. Zhang, G. Gaucher and J. C. Leroux, *Nano Lett.*, 2005, **5**, 315.

28 S. H. Kim, J. P. K. Tan, F. Nederberg, K. Fukushima, Y. Y. Yang, R. M. Waymouth and J. L. Hedrick, *Macromolecules*, 2009, **42**, 25.

29 B. H. Tan, H. Hussain, T. T. Lin, Y. C. Chua, Y. W. Leong, W. W. Tjiu, P. K. Wang and C. B. He, *Langmuir*, 2011, **27**, 10538.

30 R. Mincheva, J.-M. Raquez, V. Lison, E. Duquesne, O. Talon and P. Dubois, *Macromol. Chem. Phys.*, 2012, **213**, 643.

31 http://www.veeco.com/pdfs/appnotes/quantitative-mechanical-property-mapping-at-the-nanoscale-with-peakforce-qnm-an128-lores.pdf

32 M. Tielemans, P. Roose, C. Ngo, R. Lazzaroni and P. Leclère, *Prog. Org. Coatings*, 2012, **75**, 560.

33 M. Yasuniwa, S. Tsubakihara, K. Iura, Y. Ono, Y. Dan and K. Takahashi, *Polymer*, 2006, **47**, 7554.

34 G. Mertz, F. Hassouna, P. Leclère, A. Dahoun, D. Ruch and V. Toniazzo, *Polym. Degrad. Stab.*, 2012, **97**, 2195.

35 H. Xu, C. Teng and M. Yu, Polymer, 2006, **47**, 3922; L. Jia, L. Yin, Y. Li, Q. Li, J. Yang, J. Yu, Z. Shi, Q. Fang and A. Cao, *Macromol. Biosci.*, 2005, **5**, 526.

36 Y. Habibi, L. A. Lucia and O. J. Rojas, *Chem. Rev.*, 2010, **110**, 3479.

37 H. K. Zhao, J. H. Kwak, Y. Wang, J. A. Franz, J. M. White and J. E. Holladay, *Energy Fuels*, 2006, **20**, 807.

38 S. Gogolewski, *Coll. Polym. Sci.*, 1978, **256**, 323.

39 O. V. Borisov, E. B. Zhulina, F. A. M. Leermakers, A. H. E. Müller. In *Advances in Polymer Science*, Eds. A. H. E. Müller, O. V. Borisov, Springer-Verlag Berlin Heidelberg, 2011, **241**, 57.

40 R. Mincheva, F. Bougard, D. Paneva, M. Vachaudez, N. Manolova, P. Dubois and I. Rashkov, *J. Polym. Sci. A: Polym. Chem.*, 2008, **46**, 6712.